High Power Laser Science and Engineering, (2022), Vol. 10, e32, 7 pages.
doi:10.1017/hpl.2022.19

HIGH POWER LASER SCIENCE AND ENGINEERING

RESEARCH ARTICLE

Forty-five terawatt vortex ultrashort laser pulses from a chirped-pulse amplification system

Zhenkuan Chen[1,2,†], Shuiqin Zheng[1,2,4,†], Xiaoming Lu[3], Xinliang Wang[3], Yi Cai[1], Congying Wang[1], Maijie Zheng[1], Yuexia Ai[1], Yuxin Leng[3], Shixiang Xu[1], and Dianyuan Fan[2]

[1] *Shenzhen Key Laboratory of Micro-Nano Photonic Information Technology, Key Laboratory of Optoelectronic Devices and Systems of Ministry of Education and Guangdong Province, College of Physics and Optoelectronic Engineering, Shenzhen University, Guangzhou, China*

[2] *SZU-NUS Collaborative Innovation Center for Optoelectronic Science & Technology, Key Laboratory of Optoelectronic Devices and Systems of Ministry of Education and Guangdong Province, Shenzhen University, Guangzhou, China*

[3] *State Key Laboratory of High Field Laser Physics, Shanghai Institute of Optics and Fine Mechanics, Chinese Academy of Sciences, Shanghai, China*

[4] *Great Bay University, Dongguan, China*

(Received 29 October 2021; revised 30 June 2022; accepted 29 July 2022)

Abstract

We report on a vortex laser chirped-pulse amplification (CPA) system that delivers pulses with a peak power of 45 TW. A focused intensity exceeding 10^{19} W/cm^2 has been demonstrated for the first time by the vortex amplification scheme. Compared with other schemes of strong-field vortex generation with high energy flux but narrowband vortex-converting elements at the end of the laser, an important advantage of our scheme is that we can use a broadband but size-limited q-plate to realize broadband mode-converting in the front end of the CPA system, and achieve high-power amplification with a series of amplifiers. This method is low cost and can be easily implemented in an existing laser system. The results have verified the feasibility to obtain terawatt and even petawatt vortex laser amplification by a CPA system, which has important potential applications in strong-field laser physics, for example, generation of vortex particle beams with orbital angular momentum, fast ignition for inertial confinement fusion and simulation of the extreme astrophysical environment.

Keywords: high-power laser; light amplification; mode conversion; optical vortex

1. Introduction

The vortex laser field with orbital angular momentum[1] provides a new degree of freedom for light field manipulation and is widely applied in micrometer-scale matter manipulation[2,3], microscopy[4,5], optical communication[6,7], quantum optics[8,9] and astrophysics[10]. Nowadays, with the development of high-peak-power lasers[11–13], ultra-strong vortex laser pulses have drawn significant attention for the interaction mechanism with matter and applications in strong-field laser physics. As a consequence, some new theoretical concepts have been proposed, for example, vortex particle beam acceleration[14], strong magnetic field generation[15], the intense terahertz vortex[16], and vortex high-order harmonic generation[17]. However, the corresponding experimental verification is devoid due to the lack of a high-quality terawatt/petawatt (TW/PW) vortex laser. To realize such a vortex laser, some vortex mode-converting devices have been used, which are required to bear high energy flux and also low topological charge (TC) dispersion. High-power lasers usually have broad coherent bandwidths, and high TC dispersion will cause a problem in that in the frequency components away from the central frequency it is difficult to maintain the same TC as the central one, or the dispersion of TC will degrade the vortex purity over a broad spectral region.

However, common vortex-converting devices, such as the spiral phase plate (SPP), fork grating and q-plate, cannot

Correspondence to: Y. Cai and S. Xu, Shenzhen Key Laboratory of Micro-Nano Photonic Information Technology, Key Laboratory of Optoelectronic Devices and Systems of Ministry of Education and Guangdong Province, College of Physics and Optoelectronic Engineering, Shenzhen University, Guangzhou 518060, China. Emails: caiyi@szu.edu.cn (Y. Cai); shxxu@szu.edu.cn (S. Xu)

[†]These authors contributed equally to this work.

satisfy both requirements simultaneously. The SPP is based on phase retardation by lightwave transmission, so it is sensitive to the wavelength. The bandwidth of a reflective SPP (TC = 1) is calculated at approximately 25 nm and decreases proportionally when the TC increases if the TC deviation is less than 0.1 at 800 nm. Wang *et al.*[18] used a reflective phase plate with a size of 230 mm × 170 mm and 32 steps placed at the end of a PW laser system to generate 40-fs vortex pulses with the pulse energy up to 13 J. Unfortunately, the huge elements with the discontinuous phase distribution are with high cost, and the TC dispersion can degrade the beam quality. Leblanc *et al.*[19] proposed a plasma-based holographic grating to generate optical vortices, whose energy flux is free from optical damage. In this scheme, the plasma-based fork grating is prepared by two interfering beams, where the main beam should be incident at a proper time with a diffraction efficiency of only 6%. What is more, this technique suffers from chromatic angular dispersion. Different from the SPP and fork grating, the q-plate is a kind of wave plate with its optical axis rotating with the azimuth[20]. It can realize ultra-broadband mode conversion from 400 to 1040 nm[21] with the help of two quarter-wave plates and a polarizer. However, its small manufacturing size prevents applications in high energy flux.

Except by directly mode-converting, there is another feasible way to realize a broadband high-power vortex laser: generate a weak broadband vortex seed with a q-plate, then amplify the seed for high pulse power. This is also very challenging because the tolerance of amplification uniformity or symmetry is much more rigorous for a vortex pulse than for a Gaussian beam. Effort needs to be made to suppress the Gaussian mode, too. Nonuniform amplification can distort both the amplitude and phase, and thus degrade the singularity structure of the amplified field, which is crucial in many applications.

Researchers used different methods to amplify the vortex light. Optical parametric (chirped-pulse) amplification (OPA/OPCPA)[22–24] can amplify the vortex to the microjoule or millijoule level because of its ultra-broadband and high signal-to-noise ratio (SNR). In an OPCPA system[24], a 0.5-mJ broadband chirped vortex pulse was scaled up to 47 mJ with a 15-mm-long LiB_3O_5 crystal; the corresponding peak power is about 1 TW. However, further promotion of the output peak power may be limited by the sizes of the nonlinear optical crystals. Recently, our group has experimentally realized high-quality 1.8-mJ, 51-fs pulses from a mode-controlled regenerative amplification cavity[25] based on chirped-pulse amplification (CPA)[26] seeded with its 2-nJ seeds. However, in the cavity, the pump and the signal should be matched accurately, and the output TC cannot be flexibly changed unless by a structural modification of the cavity. Furthermore, limited by its mode sizes, the output energy by regenerative amplification is limited at the mJ level. To directly amplify vortex pulse power exceeding 1 TW, multi-pass amplification seems to be the preferred method, as it can operate with a large beam size (i.e., high power), simple mode-matching and broad bandwidth. In some designs[27,28], the Gaussian seed pulses pre-gain to microjoule level by regenerative amplification, then are converted to vortex mode by a liquid-crystal spatial light modulator (SLM) and amplified by multi-pass amplification to the millijoule level; the output peak power is only at the 10^{-2} TW level.

In this paper, we first report a vortex CPA laser system that delivers 29-fs pulses with a pulse power of 45 TW. A relativistic focused intensity exceeding 10^{19} W/cm^2 has been demonstrated for the first time by the vortex amplification scheme with an *F*/4 off-axis parabolic mirror. This design can be simply realized in an existing system by inserting an optical vortex converter (OVC) consisting of a q-plate, two quarter-wave plates and a polarizer, and beam expanders for the spatial matching between the seeds and the pumps. Here, the OVC is placed after the second amplifier to generate an 18.7-mJ vortex seed. Then, the vortex pulses are amplified by the following two-stage four-pass amplifiers. The output energy is not sensitive to TC l in our design: 1.30 J for $l = 1$ and 1.32 J for $l = 2$. Our results verify that a joule-level laser with focused intensity reaching up to the relativistic region can be realized in a multi-stage CPA system, which is expected to achieve high-quality PW vortex light fields.

2. Experimental setup and results

2.1. Experimental setup

The experiment is implemented on an existing PW system that is a modified version of that reported by Chu *et al.*[29], including a regenerative amplifier and four multi-pass amplifiers (Figure 1). We only use the front three multi-pass amplifiers of this system and the compressor. Here the seed pulses are generated in an oscillator with a pulse energy of 10 nJ, and then expanded to 1.6 ns in an all-reflective Offner-type stretcher. The stretched pulses pass through an acousto-optic programmable dispersive filter (AOPDF/Dazzler), a regenerative amplifier and a six-pass amplifier to be boosted to 20 mJ. A broadband OVC is placed at the end of the six-pass amplifier where the beam size is about 10 mm to covert the Gaussian beam to a vortex beam with a TC of 1 or 2. The vortex is then seeded into two stages of four-pass amplifiers (I & II), and thus the output energy scales up to 270 mJ and 1.8 J, respectively. After a grating compressor, the chirped vortex pulse is compressed to 29 fs with a measured reflective efficiency of 72%, which means the vortex pulse energy after the compressor is about 1.3 J.

2.2. Optical vortex conversion

The OVC consists of two quarter-wave plates (QW1 and QW2), a q-plate and a polarizer, which is based on so-called

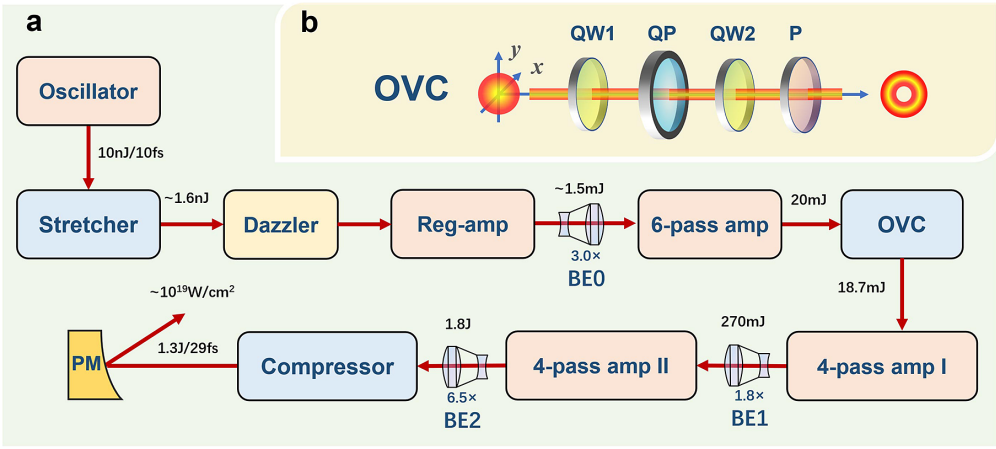

Figure 1. Schematics of the vortex CPA experimental setup (a) and the optical vortex converter (b). QW, quarter-wave plate; P, polarizer; QP, q-plate, vortex half-wave plate; OVC, optical vortex converter; BE, beam expander; PM, off-axis parabolic mirror.

spin-to-orbital angular momentum conversion, as mentioned by Marrucci *et al.*[20]. The first quarter-wave plate QW1 is used to generate a circularly polarized beam when its optical axis is oriented by 45° relative to the polarization direction of the incident laser. When this circularly polarized beam passes through the q-plate, it becomes a circularly polarized vortex beam, which is converted back to linear polarization without changing the vortex phase by the second quarter-wave plate QW2. The q-plate we used here is a vortex half-wave plate based on liquid-crystal polymer with its fast axis direction proportional to the azimuth angle. Its pulse damage threshold is as low as 0.5 J/cm^2 with 10-ns pulses, which is still an order of magnitude higher than that of the laser at the position where the OVC is placed. The TC can easily be changed by directly switching the q-plate. The near-field profiles of the beams propagating for 40 cm after the OVC are shown in Figures 2(a) and 2(d) recorded by photographic papers for $l = 1$ and 2, respectively, with the output energies of 18.7 and 18.3 mJ, corresponding to conversion efficiencies of 93.5% and 91.5%, respectively. Because the measuring position is near the OVC, the diffraction is weak, the intensity distributions of both beams are Gaussian-like with the same diameter of 10 mm, and the central dark spots are very small.

2.3. Vortex beam in amplifiers

The collimation for the beam matching between the pump and seed is more critical when using vortex seeding instead of Gaussian seeding. Incomplete matching leads to an uneven amplification that easily causes asymmetric distributions of the beams around the central dark spot. A flat-top super-Gaussian pump can help decrease the difficulty of optical alignment and improve the stability of the laser system compared to a Gaussian pump or annular pump. In four-pass amplifier I, the pump source is a frequency-doubled Nd:YAG laser that delivers a super-Gaussian mode with the size of 12 mm, pulse energy of 1 J and repetition rate of 1 Hz at 532 nm. After four-pass amplification, the pulse energy scales up to 270 and 266 mJ for $l = 1$ and 2, respectively, compared to 280 mJ for $l = 0$ for the Gaussian seed. The corresponding output near-field profiles are shown in Figures 2(b) and 2(e). As they propagate in the amplifier, the beams become doughnut-shaped for the diffraction effect. Experimentally, it is more convenient to use the bright ring diameter as the spot size of the high-order modes[30], which is 8 and 10 mm for $l = 1$ and 2, respectively, although both of them have the same profile size of 12 mm, which is consistent with pump size.

In four-pass amplifier II, to control the beam size at a proper level, we readjust the expanding ratio of the original beam expander (BE1) from 3.0× to an optimal value of 1.8×. An 80-mm-diameter Ti:sapphire is used in the stage, which is pumped by a frequency-doubled Nd:glass laser with the size of 23 mm and the energy of 7 J, which can be up to 9 J at maximum output. After four-pass amplification, the output energy of the vortex laser is about 1.80 J for $l = 1$ and 1.83 J for $l = 2$, which are measured only by replacing the q-plate with any other structure changes and realignment, compared to 2.2 J for $l = 0$ (Gaussian). The corresponding near-field characteristics at the output end are shown in Figures 2(c) and 2(f). They have a similar profile size of 23 mm with different bright ring diameters. For $l = 1$, the diameters are 11.7 mm in the horizontal direction and 9.5 mm in the vertical direction, which are 15.4 mm in the horizontal direction and 12.2 mm in the vertical direction for $l = 2$, correspondingly.

2.4. Far-field characteristics

For an optical vortex, the maintenance of the central singularity in the far-field may be significant, rather than the focal spot size. Here, we use the ring-to-center ratio, the intensity ratio of the light ring to the central dark spot, to evaluate this

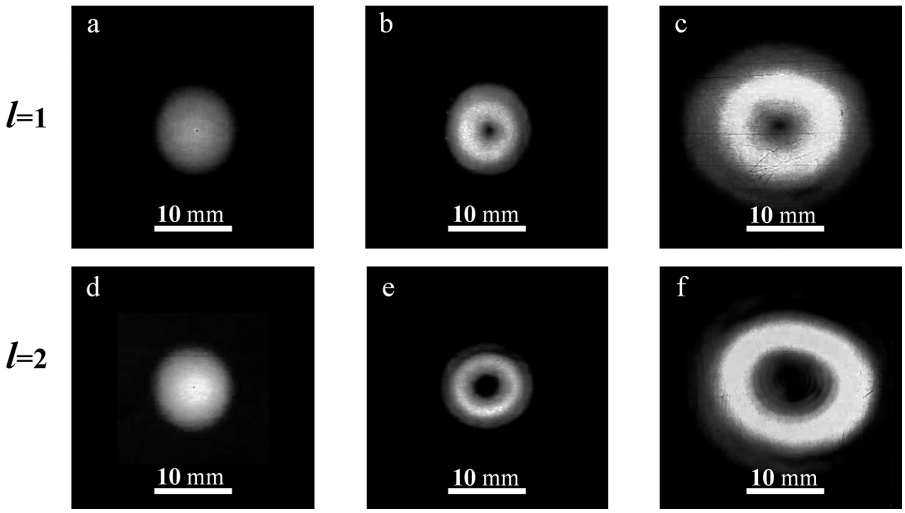

Figure 2. Near-field intensity distributions of vortex beams for topological charges $l = 1$ (upper, (a)–(c)) and 2 (lower, (d)–(f)), recorded by photographic papers. The figures correspond to the measurement places behind the OVC (left), four-pass amplifier I (middle) and four-pass amplifier II (right).

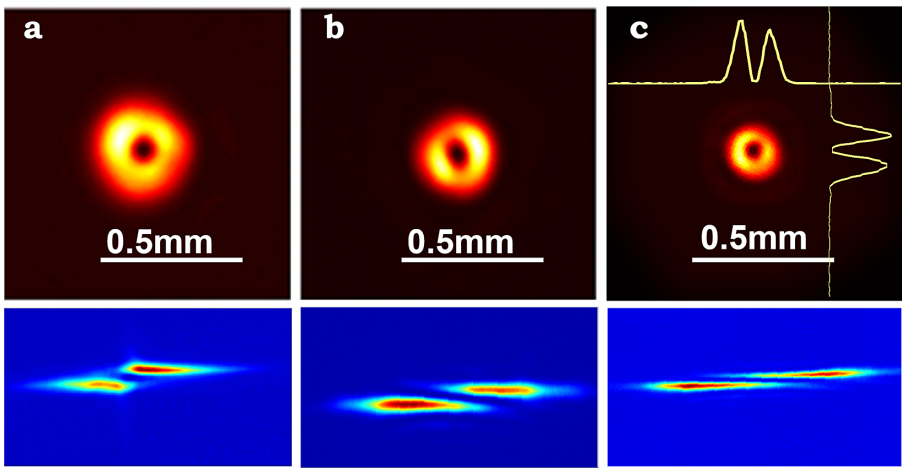

Figure 3. Far-field profiles for $l = 1$ by a spherical lens (upper) and a cylindrical lens (lower). Here, (a)–(c) correspond to Figures 2(a)–2(c), respectively.

characteristic. Many factors can impact the ring-to-center ratio, such as beam asymmetry caused by amplification nonuniformity, phase distortion caused by the *B*-integral, non-ideal suppression of the Gaussian basic mode, and the purity of the seeding caused by the finite mode-converting bandwidth of vortex-converting elements. Figures 3(a)–3(c) show the intensity profiles at the focus of a spherical lens with a focal length of 1500 mm (upper) and a cylindrical lens (lower) with a focal length of 250 mm, corresponding to three measurement positions: at the output of the OVC (left), at the four-pass amplifier I (middle) and at the four-pass amplifier II (right). As shown by the upper figures, the laser can keep its far-field as a doughnut shape well during amplification, and the diameter of the bright-ring peak is about 180, 150 or 91 μm, respectively. Comparatively, the ideal far-field diameter is calculated to be about 64 μm for a Gaussian beam with the same size as that in Figure 2(c) under the same focusing condition. The yellow curves in Figure 3(c) also show the transverse intensity distributions in both horizontal (top) and vertical (right) directions after the four-pass amplifier II. The intensity fluctuation at the bright ring between the maximum and the minimum is less than 1.6 multiples. The measured ring-to-center ratio is 13.5, or 11 dB. As we know, when an optical vortex is focused by a cylindrical lens, its far-field will show coherent $l + 1$ stripes with a TC of l. The measured high contrast of the far-fields by a cylindrical lens shows that the OVC has broad mode-converting bandwidth and the vortex characteristic of the laser phases maintains well in the amplification process.

The far-field characteristic for TC $l = 2$ are shown in Figures 4(a)–4(c) by the same spherical lens and cylindrical lens as in Figure 3. The far-fields by the spherical lens (upper) show a complete doughnut shape and those by the cylindrical lens (lower) show a clear three-fringe shape. The measured diameters of the bright-ring peak are 240,

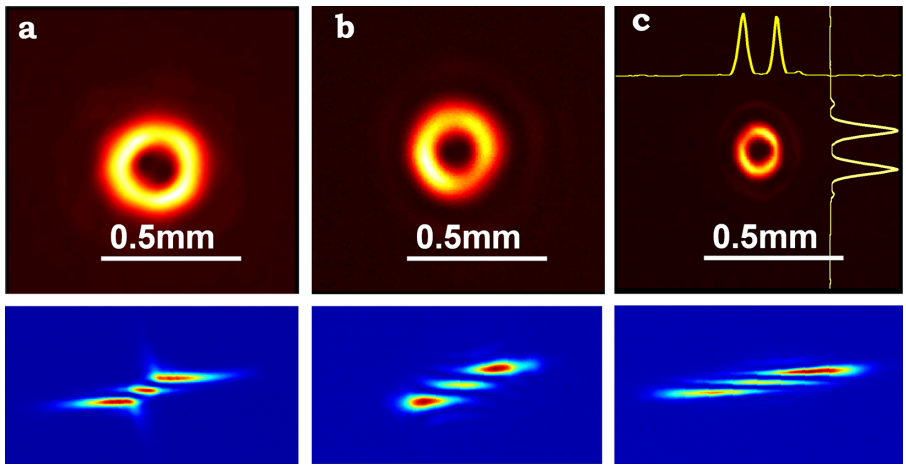

Figure 4. Far-field profiles for $l = 2$ by a spherical (upper) and a cylindrical lens (lower). Here, (a)–(c) correspond to Figures 2(a)–2(c), respectively.

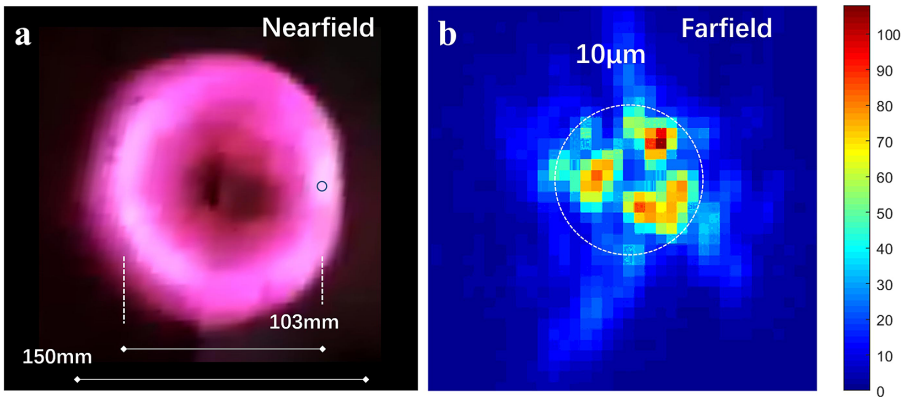

Figure 5. The spot profiles at the near-field after compression (a) and the far-field with an $F/4$ parabolic mirror (b).

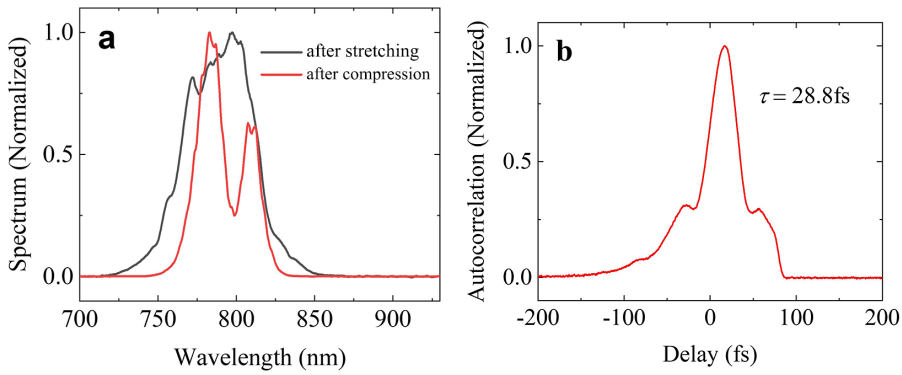

Figure 6. (a) Measured spectra after stretching (black line) and compression (red line). (b) Measured autocorrelation trace of the compressed pulse sampled in the region within the blue circle in Figure 5(a).

220, and 120 μm, respectively. This smaller far-field in Figure 4(c) compared to $l = 2$ can be attributed to its larger near-field. The ring-to-center ratio is 11, or 10 dB.

2.5. Output characteristics

After four-pass amplifier II, the beam diameter is expanded to 150 mm (profile size) to match the vacuum grating compressor and the paraboloidal mirror in the target chamber, which are designed for PW lasers originally. The near-field profile of the beam with TC $l = 1$ is shown in Figure 5(a), where the diameter of the bright ring is about 103 mm. This beam is focused with a 150-mm diameter and 600-mm focal length off-axis parabolic mirror, and the focused size is measured to be about 10 μm with approximately 50% energy within this area, as shown in Figure 5(b). The ring-to-center

ratio is about 6 dB. Unfortunately, as by Longman *et al.*[31], the obvious degradation of the far-field beam profile occurs, which, in our opinion, can be attributed to the imperfect quality and residual focusing aberrations of the parabolic mirror as well as some spatiotemporal coupling effects in the large-size compressor.

The red line in Figure 6(a) shows the output spectrum at the end of the laser, which has a saddle shape, and the spectral width (full width at half maximum, FWHM) is about 43.3 nm. This saddle shape is modulated by the Dazzler to suppress spectrum gain narrowing and control the spectral shape. Comparatively, the black line in Figure 6(a) shows the spectrum after the stretcher with a bandwidth of 50 nm. The output temporal characteristic is measured by a single-shot autocorrelator. As shown in Figure 6(b), the corresponding pulse duration is estimated to be 29 fs. The autocorrelation measurement is made to a sub-aperture (~5 mm diameter, as shown by the blue circle in Figure 5(a)) of the beam to ensure that the measured part has a relatively uniform phase distribution. The transmission efficiency of the compressor is measured as about 72%, while the output pulse energy is about 1.3 J for both $l = 1$ and 2, corresponding to a peak power of 45 TW. Within this zone, the focused intensity can be estimated as 2.7×10^{19} W/cm^2.

3. Conclusions

In this paper, we propose a simple but effective method to realize vortex ultrashort laser pulse amplification to several tens TW in an existing CPA laser system by inserting some all-transmission vortex-converting elements and pump adaptations. In our scheme, a broad mode-converting bandwidth is realized by a q-plate-based vortex converter to generate 18-mJ vortex seed pulses. The beam expanding ratio between the amplifiers is redesigned to match the seed and pump beam. After being amplified by two stages of four-pass amplifiers, the vortex pulse energy scales up to about 1.8 J for both $l = 1$ and 2, which is about 82% of that when the laser operates in super-Gaussian mode. The TC switch between 1 and 2 can be flexibly realized only by directly replacing the q-plate without realignment. The final output pulse from the compressor has an energy of 1.3 J and pulse width of 29 fs, corresponding to a peak power of 45 TW. By using an off-axis parabolic mirror with an F-number of 1/4, the focused peak intensity reaches a relativistic intensity of 2.7×10^{19} W/cm^2. The measured near- and far-field distributions show that the vortex characteristic can be well maintained in the amplification process but degrade after being compressed and focused. A vortex laser directly amplified in a CPA system is an efficient method for intense vortex laser generation and provides a powerful tool for the study of strong-field light physics, such as vortex particle acceleration[14], strong magnetic field generation[15], the relativistic vortex cutter[31], and astrophysical simulation[10]. To boost the laser to PW level, non-ideal large-size optical elements, aberrations by off-axis focusing and pulse-contrast degradation by large amplified spontaneous emission are the challenges researchers face.

Acknowledgments

This work was partly supported by the National Natural Science Foundation of China (Nos. 92050203, 61925507, 12174264, 12004261, 62075138, and 61827815), the Natural Science Foundation of Guangdong Province (Nos. 2021A1515011909 and 2022A1515011457), and the Shenzhen Fundamental Research Projects (Nos. JCYJ20200109105606426, JCYJ20190808164007485, JCYJ20190808121817100, JCYJ20190808143419622, and JCYJ2019080 8115601653).

References

1. L. Allen, M. W. Beijersbergen, R. J. C. Spreeuw, and J. P. Woerdman, Phys. Rev. A **45**, 8185 (1992).
2. M. Padgett and R. Bowman, Nat. Photonics **5**, 343 (2011).
3. L. Paterson, M. P. MacDonald, J. Arlt, W. Sibbett, P. E. Bryant, and K. Dholakia, Science **292**, 912 (2001).
4. A. Jesacher, S. Furhapter, S. Bernet, and M. Ritsch-Marte, Phys. Rev. Lett. **94**, 233902 (2005).
5. B. Jack, J. Leach, J. Romero, S. Franke-Arnold, M. Ritsch-Marte, S. M. Barnett, and M. J. Padgett, Phys. Rev. Lett. **103**, 083602 (2009).
6. J. Wang, J. Y. Yang, I. M. Fazal, N. Ahmed, Y. Yan, H. Huang, Y. X. Ren, Y. Yue, S. Dolinar, M. Tur, and A. E. Willner, Nat. Photonics **6**, 488 (2012).
7. N. Bozinovic, Y. Yue, Y. X. Ren, M. Tur, P. Kristensen, H. Huang, A. E. Willner, and S. Ramachandran, Science **340**, 1545 (2013).
8. A. Mair, A. Vaziri, G. Weihs, and A. Zeilinger, Nature **412**, 313 (2001).
9. D. Cozzolino, E. Polino, M. Valeri, G. Carvacho, D. Bacco, N. Spagnolo, L. K. Oxenløwe, and F. J. A. P. Sciarrino, Adv. Photonics **1**, 046005 (2019).
10. F. Tamburini, B. Thide, G. Molina-Terriza, and G. Anzolin, Nat. Phys. **7**, 195 (2011).
11. C. N. Danson, C. Haefner, J. Bromage, T. Butcher, J.-C. F. Chanteloup, E. A. Chowdhury, A. Galvanauskas, L. A. Gizzi, J. Hein, D. I. Hillier, N. W. Hopps, Y. Kato, E. A. Khazanov, R. Kodama, G. Korn, R. Li, Y. Li, J. Limpert, J. Ma, C. H. Nam, D. Neely, D. Papadopoulos, R. R. Penman, L. Qian, J. J. Rocca, A. A. Shaykin, C. W. Siders, C. Spindloe, S. Szatmári, R. M. G. M. Trines, J. Zhu, P. Zhu, and J. D. Zuegel, High Power Laser Sci. Eng. **7**, e54 (2019).
12. J. W. Yoon, C. Jeon, J. Shin, S. K. Lee, H. W. Lee, I. W. Choi, H. T. Kim, J. H. Sung, and C. H. Nam, Opt. Express **27**, 20412 (2019).
13. A. Shaykin, V. Ginzburg, I. Yakovlev, A. Kochetkov, A. Kuzmin, S. Mironov, I. Shaikin, S. Stukachev, V. Lozhkarev, A. Prokhorov, and E. Khazanov, High Power Laser Sci. Eng. **9**, e54 (2021).
14. M. Kozák, ACS Photonics **8**, 431 (2021).
15. Y. Shi, J. Vieira, R. M. G. M. Trines, R. Bingham, B. F. Shen, and R. J. Kingham, Phys. Rev. Lett. **121**, 145002 (2018).

16. H. G. Wang, Q. Y. Song, Y. Cai, Q. G. Lin, X. W. Lu, H. C. Shangguan, Y. X. Ai, and S. X. Xu, Chin. Phys. B **29**, 097404 (2020).
17. L. Rego, K. M. Dorney, N. J. Brooks, Q. L. Nguyen, C.-T. Liao, J. S. Román, D. E. Couch, A. Liu, E. Pisanty, M. Lewenstein, L. Plaja, H. C. Kapteyn, M. M. Murnane, and C. Hernández-García, Science **364**, 1253 (2019).
18. W. P. Wang, C. Jiang, H. Dong, X. M. Lu, J. F. Li, R. J. Xu, Y. J. Sun, L. H. Yu, Z. Guo, X. Y. Liang, Y. X. Leng, R. X. Li, and Z. Z. Xu, Phys. Rev. Lett. **125**, 034801 (2020).
19. A. Leblanc, A. Denoeud, L. Chopineau, G. Mennerat, P. Martin, and F. Quéré, Nat. Phys. **13**, 440 (2017).
20. L. Marrucci, C. Manzo, and D. Paparo, Phys. Rev. Lett. **96**, 163905 (2006).
21. M. Gecevicius, M. Ivanov, M. Beresna, A. Matijosius, V. Tamuliene, T. Gertus, A. Cerkauskaite, K. Redeckas, M. Vengris, V. Smilgevicius, and P. G. Kazansky, J. Opt. Soc. Am. B **35**, 190 (2018).
22. P. Stanislovaitis, M. Ivanov, A. Matijosius, V. Smilgevicius, and T. Gertus, Opt. Eng. **56**, 095101 (2017).
23. K. Yamane, Y. Toda, and R. Morita, Opt. Express **20**, 18986 (2012).
24. W. J. Pan, X. Y. Liang, L. H. Yu, A. T. Wang, J. F. Li, and R. X. Li, IEEE Photonics J. **12**, 1502608 (2020).
25. S. Q. Zheng, Z. K. Chen, Q. G. Lin, Y. Cai, X. W. Lu, Y. X. Gao, S. X. Xu, and D. Y. Fan, Photonics Res. **8**, 1375 (2020).
26. D. Strickland and G. Mourou, Opt. Commun. **56**, 219 (1985).
27. Y. C. Lin, Y. Nabekawa, and K. Midorikawa, Appl. Phys. B **122**, 280 (2016).
28. K. Yamane, A. Honda, Y. Toda, and R. Morita, in *19th International Conference on Ultrafast Phenomena* (Optical Society of America, Okinawa, 2014), paper 08.Tue.D.5.
29. Y. X. Chu, X. Y. Liang, L. H. Yu, Y. Xu, L. Xu, L. Ma, X. M. Lu, Y. Q. Liu, Y. X. Leng, R. X. Li, and Z. Z. Xu, Opt. Express **21**, 29231 (2013).
30. J. T. Luxon, and D. E. Parker, Appl. Opt. **20**, 1728 (1981).
31. A. Longman, C. Salgado, G. Zeraouli, J. I. Apiñaniz, J. A. Pérez-Hernández, M. K. Eltahlawy, L. Volpe, and R. Fedosejevs, Opt. Lett. **45**, 2187 (2020).